Int. J. Electrochem. Sci., 13 **(2018)** 4720 – 4730, doi: 10.20964/2018.05.29

International Journal of
ELECTROCHEMICAL
SCIENCE
www.electrochemsci.org

One-step Convenient Hydrothermal Synthesis of MoS_2/RGO as a High-performance Anode for Sodium-ion Batteries

Haishen Song[1,2,*], *Anping Tang*[1], *Guorong Xu*[2], *Lihua Liu*[3], *Mengjia Yin*[2], *and Yijin Pan*[2]

[1] Key Laboratory of Theoretical Organic Chemistry and Functional Molecule, Ministry of Education
[2] School of Chemistry and Chemical Engineering, Hunan University of Science and Technology, Xiangtan 411201, PR China
[3] Hunan Province College Key Laboratory of QSAR/QSPR
[*]E-mail: Song_shs@126.com

Received: 17 January 2018 / *Accepted:* 1 March 2018 / *Published:* 10 April 2018

A molybdenum disulfide (MoS_2) nanosheet was grown directly on a surface of reduced graphene oxide (RGO) by using a one-step hydrothermal growth technique. The samples were systematically characterized by using X-ray diffraction (XRD), field-emission scanning electron microscopy (FE-SEM) and high-resolution transmission electron microscopy (HRTEM). The electrochemical properties were evaluated by cyclic voltammetry, galvanostatic charge/discharge and electrochemical impedance spectroscopy tests in two-electrode cells. The results indicate that the synthesized MoS_2/RGO composites show excellent electrochemical performance as anode materials for Na-ion batteries. The MoS_2/RGO composites exhibit an initial discharge capacity of 715.5 mAh g^{-1} and an initial charge capacity of 440.5 mAh g^{-1} at a current density of 100 mA g^{-1}. The composites also exhibit excellent cycling stability with almost no capacity fading after 100 cycles at a current density of 250 mA g^{-1} compared with only 39.6% of that for pure MoS_2, and the electrode shows stable high-rate performance. The superior electrochemical performance of the MoS_2/RGO composites as Na-ion battery anodes may be attributed to their loose structure and the excellent conductivity of reduced graphene oxide in MoS_2/RGO.

Keywords: MoS_2/RGO composites; hydrothermal synthesis; anode material; sodium-ion battery

1. INTRODUCTION

Due to the scarcity of lithium, there are clear and compelling economic and practical drivers to explore alternatives to lithium ions in charge storage devices[1,2,3]. Sodium-ion batteries (SIBs) have many advantages due to the intrinsic advantages of sodium, for example, they are environmentally benign, easy to recover, inexpensive and relatively abundant[4,5,6]. However, the larger ion radius and

transport barrier restrict the choice of electrode materials for SIBs[7,8]. Therefore, it is of great importance to explore a suitable host for SIBs.

Molybdenum disulfide (MoS_2) has a similar layered structure to graphite, in which each layer has a slab of transition metal atoms sandwiched by two slabs of chalcogenide atoms. Covalent bonds are formed between Mo and S within each layer and the Mo-S polyhedron can be described as a trigonal prism where Mo^{4+} is in the centre of the prism[9,10]. In the structure, adjacent MoS_2 layers are interconnected with weak van der Waals forces, and there is sufficient space between the layers to host alkali metal ions during charging, which suggests the possibility of MoS_2 as a potential electrode material for high-capacity rechargeable batteries. However, bulk MoS_2 possesses low conductivity and suffers from large volume expansion and pulverization when used as an anode material, which render poor cycle performance and poor rate capability[9,11]. To overcome these problems and improve the electrochemical properties of MoS_2, various strategies have been proposed, and one effective approach is to design composites with a matrix that can act as a buffer layer for volume expansion during charge-discharge processes[11,12,13,14]. Among those materials, graphene sheets have been considered as a potential matrix material to improve the electrochemical performance of MoS_2 due to their extraordinary electronic transport properties, large surface area and mechanical flexibility[15,16].

Previous studies have synthesized MoS_2/G by various methods, and most of the methods contain complex steps[17,18]. To modify the interlayer structure of MoS_2 and accelerate both electron and ion transport in a simple way, we produced layered MoS_2/RGO composites using a one-step hydrothermal method. The results demonstrated that the obtained MoS_2/RGO composites show excellent electrochemical performance as anode materials for sodium-ion batteries compared with bulk MoS_2 due to the synergistic effects between layered MoS_2 and graphene. The MoS_2/RGO composites present a high rate stability and an excellent cycling stability with almost no capacity fading after 100 cycles at a current density of 250 mA g^{-1}.

2. EXPERIMENTAL

2.1 Synthesis of the MoS_2/RGO composites

Graphene oxide (GO, 20 mg) synthesized by a modified Hummers method was dispersed in 60 ml of ultrapure water under vigorous ultrasonic agitation to form a homogeneous solution. Then, 1.5 g of sodium molybdate and 1.9 g of thiourea were added into the above dispersion successively. After ultrasonication and stirring for 20 min, the solution was transferred into a 100 ml Teflon-lined stainless steel autoclave, sealed tightly and then hydrothermally treated at 180℃ for 24 h. After cooling naturally, the resulting black precipitate was collected by filtering and washing with ultrapure water and absolute ethanol for several times and dried in a vacuum oven at 80℃ for 12h. Then, the MoS_2/RGO composites were obtained. For comparison, MoS_2 was also synthesized through similar procedures without adding GO.

2.2 Material characterization

X-ray diffractometer (Bruker D-8) (Cu Kα, l=0.154056 nm) was applied to study the phase structure of samples. Field emission scanning electron microscopy (FESEM, JSM-6360LV, JEOL) and high-resolution transmission electron microscopy (HRTEM, Tecnai G2F20 S-TWIX) were used to determine the morphology of the as-prepared composites. Raman spectra (LabRAM HR800) were obtained with a laser excitation of 532 nm.

2.3 Electrochemical measurements

The electrochemical properties were studied by using two-electrode cells that were assembled in an argon-filled glove box. The electrodes were prepared by mixing the prepared active material, acetylene black and sodium alginate (7:2:1 wt/wt/wt) in water to obtain a uniform slurry. The slurry was coated onto a copper foil and dried in a vacuum oven at 80 ℃ overnight. The CR2032 coin cells were assembled in an argon-filled glove box using a glass microfibre (Whatman) membrane and sodium metal foil as the separator and counter electrodes, respectively. The electrolyte was a mixture of 1 M $NaClO_4$ in EC/DMC (1:1, vl/vl) with 5 wt% fluoroethylene carbonate (FEC). Galvanostatic charge/discharge measurements were carried out in the voltage range of 0.01 ~ 3.00 V on a battery tester at various current densities. Cyclic voltammetry measurements were performed on an electrochemical workstation within the voltage range of 0.01-3.00 V at a scan rate of 0.2 mV/s. Electrochemical impedance spectroscopy (EIS) data were measured applying a 5 mV amplitude signal in the frequency range of 100 kHz to 0.01 Hz. The specific capacity of the electrode was calculated based on the total mass of MoS_2/RGO synthesized in the experiment.

3. RESULTS AND DISCUSSION

The XRD patterns of pure MoS_2 and MoS_2/RGO are presented in Figure 1. As shown in the Figure, MoS_2 exhibits high crystallinity, and the diffraction peaks observed at 14.1°, 33.3°, 44.4° and 58.65° correspond to different crystal planes of hexagonal MoS_2, which is in accordance with those established by JCPDS card number 37-1492[19,20,21]. The strong peak at 14.1° corresponds to the (002) plane with a d-spacing of 0.63 nm, indicating that layered MoS_2 grows well along the c axis during synthesis[11]. In addition, the MoS_2/RGO composites basically retain the layered crystallinity and the position of the diffraction peaks of MoS_2[18]. However, it is worth noting that the intensity of the (002) plane peak of MoS_2 decreases with the addition of graphene in the composites, which indicates that the incorporation of the graphene considerably inhibits the (002) plane growth of MoS_2 crystals in the composites. Additionally, the XRD pattern of the MoS_2/RGO composites shows that the (002) diffraction peak of the graphene nanosheets cannot be detected, indicating that the graphene nanosheets do not stack during the hydrothermal process[18].

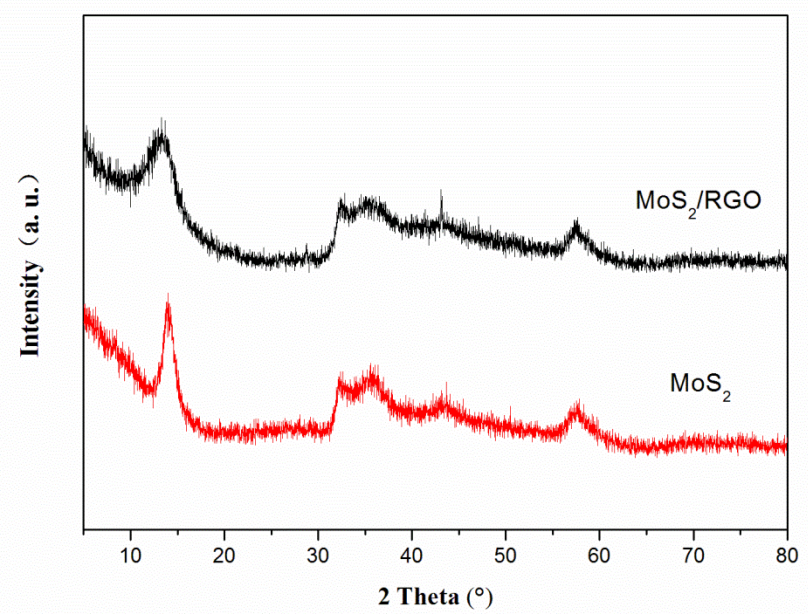

Figure 1. XRD patterns of pure MoS_2 and MoS_2/RGO

The morphologies of MoS_2 and MoS_2/RGO are characterized using SEM. It can be seen from Figure 2 that bare MoS_2 obtained through the proposed method aggregates severely and consists of large-scale sheets that are tightly stacked together. A nucleation of MoS_2 occurs during the hydrothermal process, and a subsequent accumulation occurred directly on the substrate surface. Moreover, increases in the reaction time turned MoS_2 nucleation into a nanosheet-like structure, and the addition of GO highly affects the morphology of the material. When GO was predispersed in the hydrothermal solution, the microsized MoS_2/RGO composites displayed a loose 3D architecture morphology consisting of a large number of scaled and curved sheets, as shown in Figure 2b. The 3D architecture of the MoS_2/RGO composites was caused by graphene self-assembling during the hydrothermal process, in which GO was reduced to graphene, and the flexible graphene self-assembled into a 3D architecture by partial overlapping or coalescing of the sheets[18]. It is demonstrated that MoO_4^{2-} was reduced to MoS_2 by thiourea, and GO was reduced to graphene simultaneously during the hydrothermal process. Thiourea plays the role of a reducing agent and a sulfur donor during the hydrothermal process[22,23,24].

$$4Na_2MoO_4+15CS(NH_2)_2+6H_2O\rightarrow 4MoS_2+Na_2SO_4+6NaSCN+24NH_3(g)+9CO_2(g)$$

During this process, the GO or reduced GO nanosheets could be used as a novel substrate for the nucleation and subsequent growth of MoS_2[25]. The growth of MoS_2 is mainly selective on GO, attributing to the interaction between the oxygen-containing functional groups on the GO sheets and Mo precursors[26]. Due to the layered MoS_2 growth on surface of GO or reduced GO, the stacking of the graphene was inhibited during the hydrothermal process. Meanwhile, the incorporation of the reduced graphene oxide also restrained the (002) plane growth of the MoS_2 crystals in the composites[18].

Three-dimensional architectural MoS_2/RGO composites as NIB anodes will increase the contact area between the material and electrolyte, and provide more and shorter Na-ion diffusion paths

during the intercalation/deintercalation processes. In addition, the overlapping or coalescing of the graphene will form an interconnected conducting network, which is very important for the less-conducting MoS_2 as electrode materials, and facilitate rapid electronic transport during electrode reactions[18]. Finally, this 3D structure also enhances the stability of the MoS_2/RGO composites due to the super strength of graphene.

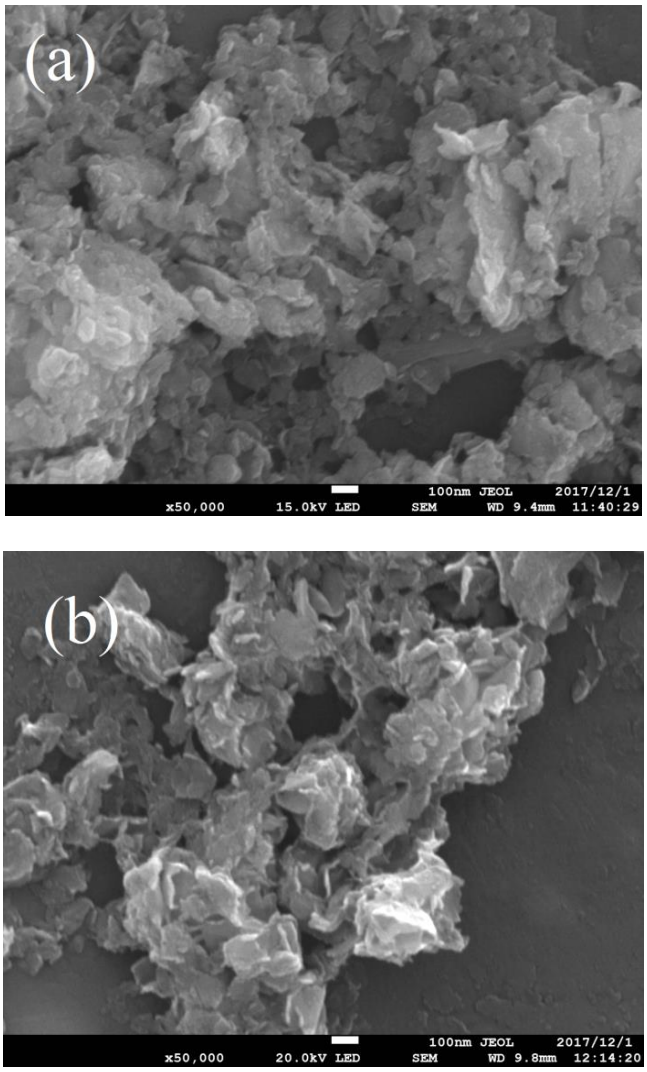

Figure 2. SEM images of MoS_2 (a) and MoS_2/RGO (b)

Subsequently, we have analysed the microstructure of the MoS_2/RGO sample in detail with high-resolution transmission electron microscopy (HRTEM), as shown in Figure 3. From Figure 3a, it can be clearly seen that layered MoS_2/RGO shows a flower-like morphology, and the MoS_2/RGO nanosheets are only a few atomic layers in thickness with an interlayer distance of 0.63 nm (Figure 3b), while pure MoS_2 shows dozens of atomic layers (Figure 3c). This few-atomic-layer thick structure is beneficial for the fast kinetics of the intercalation/deintercalation of sodium ions[11]. The selected-area electron diffraction pattern is shown in Figure 3d, and it is well-indexed as a pure hexagonal MoS_2 phase.

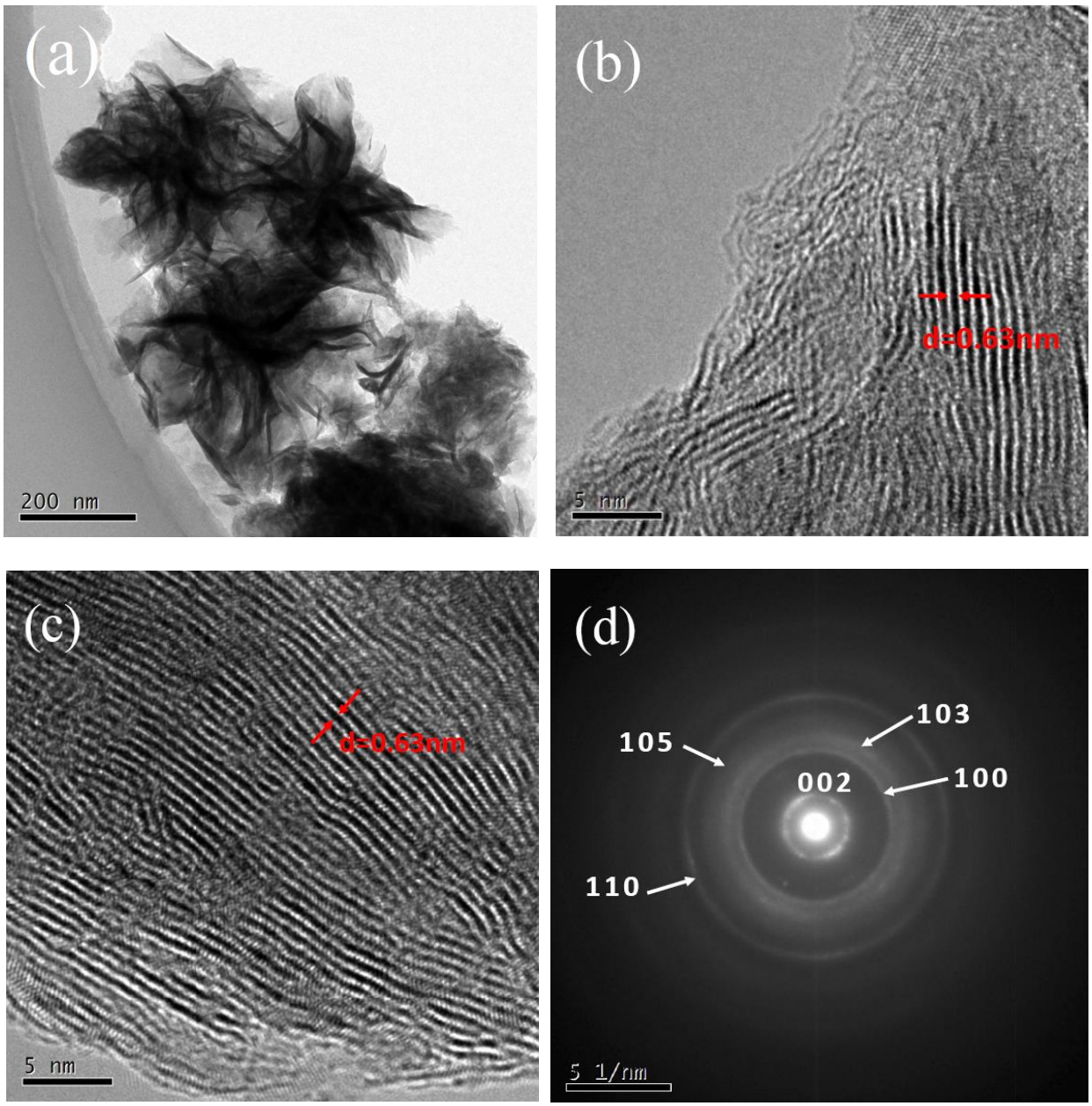

Figure 3. TEM images of MoS_2/RGO (a,b) and pure MoS_2 (c); Electron diffraction pattern of MoS_2/RGO (d)

The Raman spectra of MoS_2 and MoS_2/RGO are displayed in Figure 4. Two distinct peaks centred at approximately 1360 cm^{-1} and 1590 cm^{-1} in Raman spectra of MoS_2/RGO arise from disordered and graphic carbon further and demonstrates the existence of graphene in MoS_2/RGO[11,27]. Two other characteristic peaks located at approximately 375 cm^{-1} and 405 cm^{-1} that correspond to MoS_2 are well distinguished[11]. In addition, two distinct peaks of pure MoS_2 are detected in the Raman spectra, while the widened diffraction peak at approximately 1590 cm^{-1} may come from carbon residue in thiourea, which is in good accordance with the synthesis process.

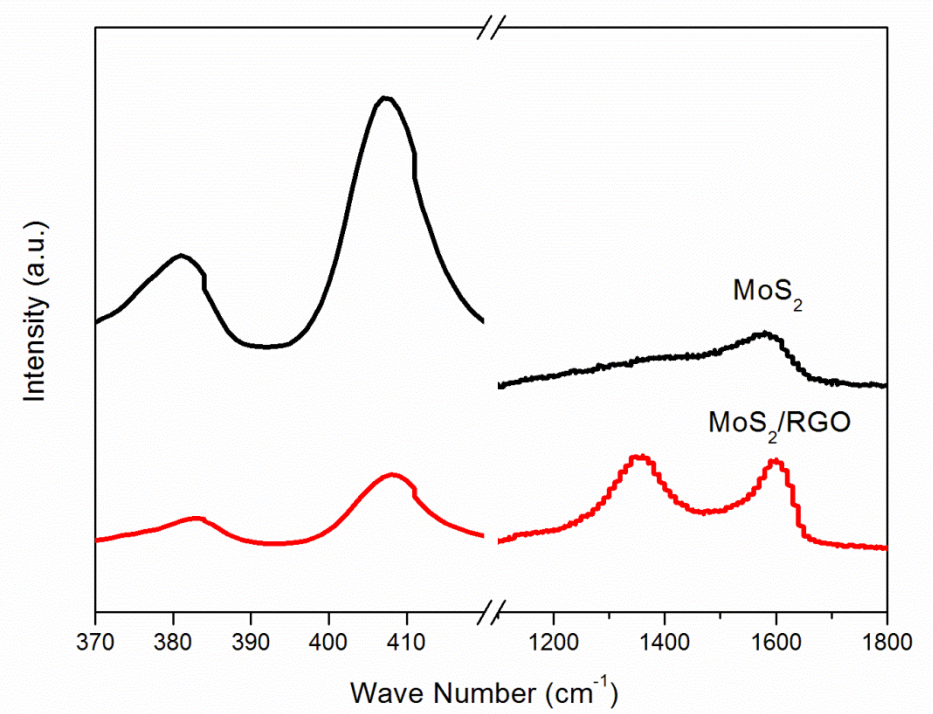

Figure 4. Raman spectra of MoS_2 and MoS_2/RGO

Experimental characterization revealed that the MoS_2/RGO composites exhibit a composite structure of layered MoS_2 and graphene. Then, the electrochemical behaviours of MoS_2/RGO are first evaluated by cyclic voltammetry (CV) measurements. As displayed in Figure 5a, the peak located at approximately 0.80 V in the first cycle corresponds to the insertion of Na^+ into MoS_2 and formation of an SEI (solid electrolyte interphase) layer. In addition, the peak located at approximately 0.1 V can be attributed to the formation of Mo and Na_2S. The anodic peak located at approximately 1.8 V is attributed to oxidation reaction from Mo to MoS_2[11]. The anodic curves during subsequent cycles show similar characteristics to that of the first cycle, while the cathodic curves show differences, which can be attributed to the formation of an SEI film at the first cycle[11]. The CV curves at the third cycle are similar to those at the second cycle, demonstrating the good reversibility of the MoS_2/RGO composite.

Figure 5b illustrates the first three charge and discharge curves of the synthesized MoS_2/RGO composites at a current density of 100 mA g^{-1}. These curves illustrate that the initial discharge capacity of MoS_2/RGO is 715.5 mAh g^{-1}, and the initial charge capacity is 440.5 mAh g^{-1}. It can be seen from the curves that two potential plateaus at approximately 1.2 V and 0.2 V are observed for the synthesized MoS_2/RGO electrode during the first discharge process, and one plateau at 1.8 V in the first charge process is observed. The charge-discharge profiles curves in the third cycle are similar to those during the second cycle, which also demonstrates good reversibility of the MoS_2/RGO composites. These results are in good agreement with the CV results. These observations are in concert with former results[11,28]. The slightly lower reductive peak of 0.80 V in the CV curves compared with that of 1.2 V in first charge-discharge profile may come from a larger current and subsequently a larger polarity during the CV measurement.

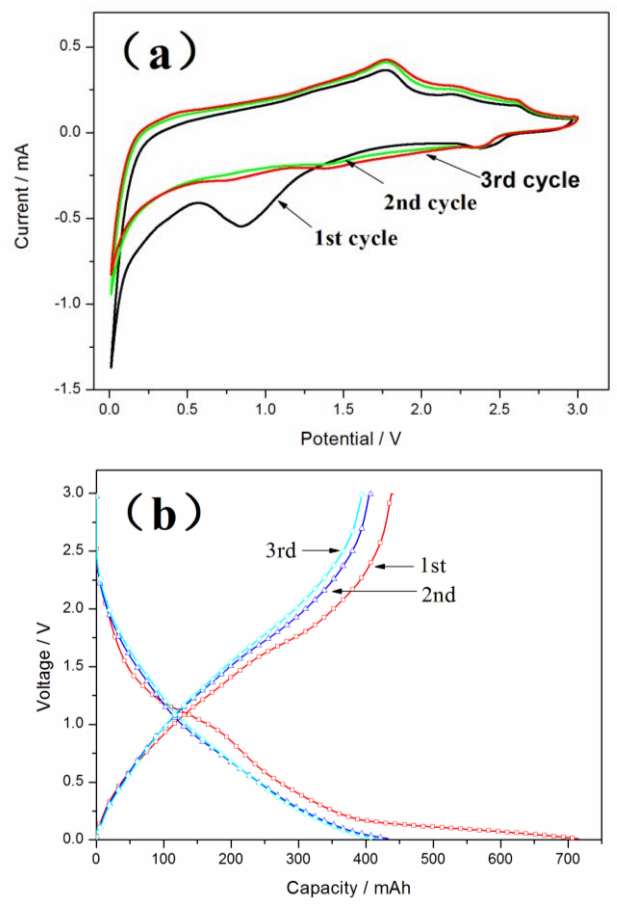

Figure 5. Cyclic voltammetry curves of the MoS_2/RGO (a) and the first three charge and discharge curves of MoS_2/RGO (b)

The cycling performances of the MoS_2 and MoS_2/RGO are tested at a current density of 250 mA g^{-1} and are illustrated. As shown in Figure 6a, the cyclic stability of MoS_2 is so poor that the reversible capacity decreases to 125 mAh g^{-1} after 100 cycles, which is only 39.6% of the initial capacity. In contrast, the MoS_2/RGO composites present an excellent cycling stability. The reversible capacity of MoS_2/RGO increases slightly during the initial dozens of cycles with almost no fading after 100 cycles. The result is consistent with earlier studies[26,27]. Thus, the incorporation of graphene largely improves their cyclic stabilities due to the robust composite structure and the synergistic effect between the layered MoS_2 and graphene[18]. In addition, the worse cycling stability of MoS_2 may be because of its tight stacking with each other, thus leading to longer sodium-ion diffusion paths.

The high reversible capacity of the MoS_2/RGO composites is also exhibited in the rate capability. Figure 6b shows the rate behaviour of the composites. At a current density of 250 mA g^{-1}, MoS_2/RGO shows a reversible capacity of 338 mA h g^{-1}. At current densities of 500 and 1000 mA g^{-1}, the reversible capacities are maintained at 280 and 240 mA h g^{-1}, respectively. Even at high current densities of 1500 mA g^{-1} and 2000 mA g^{-1}, the specific capacities remain at preferred values. When the charge/discharge current density changes from 2000 to 250 mA g^{-1}, the specific capacity of the composites returns to more than 300 mA h g^{-1}, indicating high reversibility.

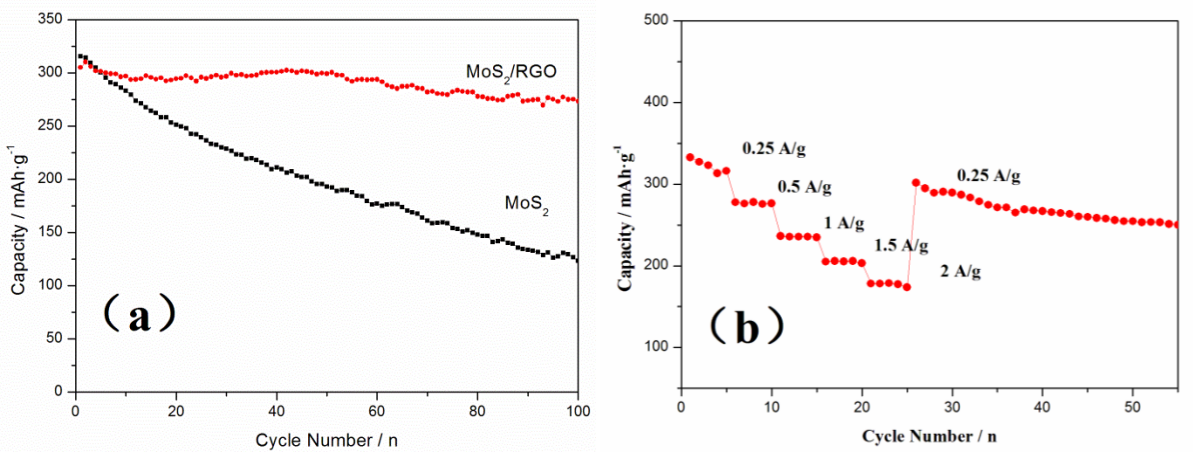

Figure 6. Cycling behaviours of MoS_2 and MoS_2/RGO at a current density of 250 mA g^{-1} (a) and rate capabilities of a MoS_2/RGO sample at different current densities (b)

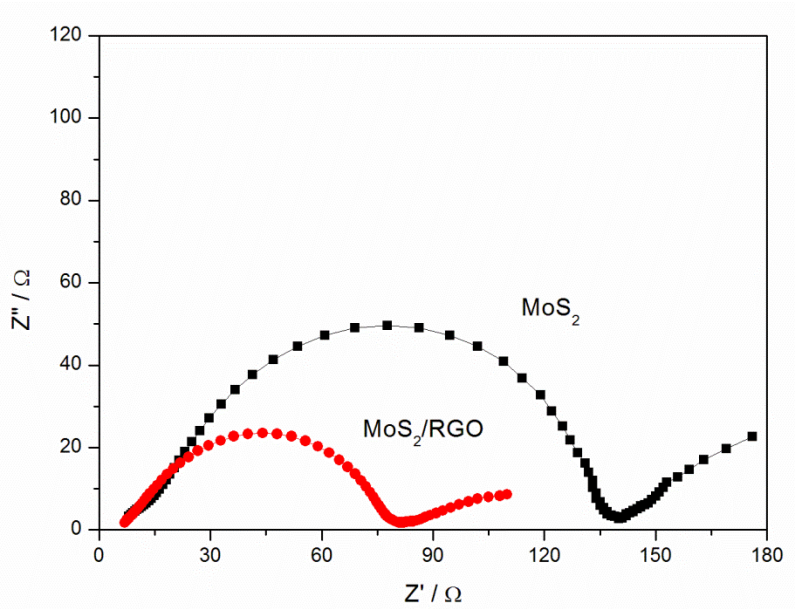

Figure 7. Nyquist plots of MoS_2 and MoS_2/RGO

To understand why the MoS_2/RGO electrode exhibits such a superior electrochemical performance, ac impedance measurements were performed after 3 cycles, as shown in Figure 7. The impedance spectra present a semicircular arc at middle frequencies and a sloped-line-like diffusion behaviour at low frequencies. The depressed semicircular arc is related to the capacitive behaviour with a parallel resistance on the electrode/electrolyte interface, for instance, a double-layer capacitance with a parallel charge transfer resistance and capacitance of an SEI layer in parallel with its resistance[29]. In addition, the inclined line corresponds to a sodium-diffusion process within the bulk of the electrode material. The middle-frequency arc width (R_w) values decrease with the addition of graphene, and the large decrease in R_w can be interpreted as a decrease in the interfacial resistance that is induced by the convenient charge transition on the MoS_2/RGO anode. This fact confirms that the incorporation of graphene can preserve the high conductivity of the MoS_2/RGO composite electrode

and greatly improve rapid electron transport during the electrochemical sodium insertion/extraction reaction, resulting in a significant improvement in the electrochemical performance. Thus, this novel type of MoS_2/RGO composite with a high reversible capacity, excellent cyclic stability, and high-rate capability demonstrates wide applications as promising anode materials for SIBs.

4. CONCLUSIONS

A convenient process was developed to synthesize layered MoS_2/RGO composites by a one-step hydrothermal method. The characterizations demonstrate that layered MoS_2 is generated on the graphene surface, which then forms a MoS_2/RGO composite. The addition of graphene inhibits the growth of layered MoS_2 crystals in the composites. The MoS_2/RGO composites exhibit a 3D architecture morphology consisting of curved nanosheets, which is attributed to the self-assembly of a graphene hydrogel during the hydrothermal process. The electrochemical evaluations reveal that the MoS_2/RGO composite electrode exhibits greater cyclic stability than does a bare MoS_2 electrode. The MoS_2/RGO composites present an excellent cycling stability with almost no capacity fading after 100 cycles at a current density of 250 mA g^{-1} compared with only 39.6% of that for MoS_2. Even at a high current density of 2000 mA g^{-1}, MoS_2/RGO exhibits an excellent cycling stability. The results confirm that the incorporation of graphene preserves the high conductivity and greatly enhances the electrochemical activity of the MoS_2/RGO composites. The improved performance is because of the looser structure of the composites and the high conductivity of reduced graphene oxide, which can accelerate the ion and electron transport, thus providing a fast kinetics mechanism for the electrochemical reactions. Therefore, the prepared MoS_2/RGO composites and the simple one-step method should be attractive for sodium ion batteries.

ACKNOWLEDGEMENTS
This work was supported by the Research Foundation of Education Bureau of Hunan Province, China (15C0532).

References

1. P. Vassilaras, S. T. Dacek, H. Kim, T. T. Fister,S. Kim, G. Ceder and J. C. Kim, *J. Electrochem. Soc.*, 164 (2017) A3484.
2. L. M. Wang, Y. Z. Liu, X. Chen, H. G. Qin and Z. H. Yang, *J. Electrochem. Soc.*, 164(2017)A3692.
3. S. L. Chou and Y. Yu, *Adv. Energy Mater.*, 7(2017)1703223.
4. Y. Xie, H. C. Wang, R. Liu, Z. G. Wang, W. Wen, Z. Jiang, Z. L. Gong and Y. Yang, *J. Electrochem. Soc.*, 164 (2017)A3487.
5. C. Nithya and S. Gopukumar, *Wiley interdisciplinary reviews: Energy and environment*, 4(2015)253.
6. N. Yabuuchi, K. Kubota, M. Dahbi and S. Komaba, *Chem. Rev.*, 114(2014)11636.
7. S. –W. Kim, D. –H. Seo, X. H. Ma, G. Ceder and K. Kang, *Adv. Energy Mater.*, 2(2012)710.

8. H. Su, S. Jaffer and H. J. Yu, *Energy Storage Materials*, 5 (2016)116.
9. Q. Q. Li, Z. P. Yao, J. S. Wu, S. Mitra, S. Q. Hao, T. S. Sahu, Y. Li, C. Wolverton and V. P. Dravid, *Nano Energy*, 38 (2017)342.
10. W. Xu, T. Wang, S. D. Wu and S. Wang, *J. Alloy. Compd.*, 698 (2017)68.
11. P. Zhang, F. R. Qin, L. Zou, M. R. Wang , K. Zhang, Y. Q. Lai and J. Li, *Nanoscale*, 9(2017)12189.
12. B. Ahmed, D. H. Anjum, M. N. Hedhili and H. N. Alshareef, *Small*, 11(2015)4341.
13. D. B. Xiao, J. Y. Zhang, X. Li, D. Zhao, H. Y. Huang, J. L. Huang, D. X. Cao, Z. H. Li and C. M. Niu, *ACS Nano*, 10(2016)9509.
14. Y. L. Jia, H. Q. Wan, L. Chen, H. D. Zhou and J. M. Chen, *J. Power Sources*, 354 (2017)1.
15. X. F. Zhou, Z. Wang, W. X. Chen, L. Ma, D. Y. Chen and J. Y. Lee. *J. Power Sources*, 251(2014)264.
16. Y. C. Liu, L. Z. Fan and L. F. Jiao, *J. Power Sources*, 340 (2017)104.
17. T. M. Masikhwa, M. J. Madito, A. Bello, J. K. Dangbegnon and Nc. Manyala, *J Colloid Interf Sci*, 488 (2017) 155.
18. K. Chang, and W. X. Chen, *ACS Nano*, 5 (2011)4720.
19. H. S. S. Ramakrishna Matte, A. Gomathi, A. K. Manna, D.J. Late, R. Datta, S. K. Pati and C. N. R. Rao, *Angewandte Chemie*, 122 (2010)4153.
20. K. Chang, Z. W. Mei, T. Wang, Q. Kang, S. X. Ouyang and J. H. Ye, *ACS Nano*, 8(2014)7078.
21. Y. R. Cui, J. S. He, X. M. Li, J. X. Zhao, A. L. Chen and J. Yang, *Adv. Mater. Res.*, 631(2013)306.
22. Q. Jiang, X. Chen, L. Li, C. Q. Feng and Z. P. Guo, *J. Electron. Mater.*, 46(2017)1079.
23. H. Zhang, X. J. Lv, Y. M. Li, Y. Wang and J. H. Li, *ACS Nano*, 4(2009)380.
24. Y. Tian, Y. He, J. Shang and Y. F. Zhu, *Acta Chim. Sinica*, 62(2004)1807.
25. Y. G. Li, H. L. Wang, L. M. Xie, Y. Y. Liang, G. S. Hong and H. J. Dai, *J. Am. Chem. Soc.*, 133(2011)7296.
26. Y. Yuan, F.F. Huang, A.Q. Pan and W. Xiao, Int. *J. Electrochem. Sci.*, 12 (2017) 5431.
27. S. Li, Zhigao Luo, X.X. Cao, G.Z. Fang and S.Q. Liang, *Int. J. Electrochem. Sci.*, 13 (2018) 23
28. X. Li, J.H. Li, Q.S. Gao, X. Yu, R.Z. Hu, J. Liu, L.C. Yang and M. Zhu, *Electrochim. Acta*, 254 (2017) 172
29. H. S. Song, Z. Cao, H. Lu, M. Jia, Z. A. Zhang, Y.Q. Lai, J. Li and Y. X. Liu, *J. Solid State Electr.*, 17(2013)599.